Published in final edited form as:
Magn Reson Med. 2012 January ; 67(1): 20–26. doi:10.1002/mrm.22993.

In Vivo Determination of Human Breast Fat Composition by 1H MRS at 7T

Ivan E. Dimitrov[*,§§], **Deborah Douglas**[*], **Jimin Ren**[*,†], **Nadine B. Smith**[%], **Andrew G. Webb**[¥], **A. Dean Sherry**[*,†,**], and **Craig R. Malloy**[1,*,†,§,††]

[*]Advanced Imaging Research Center, University of Texas Southwestern Medical Center, Dallas, Texas 75235 [§§]Philips Medical Systems, Cleveland, Ohio 44143 [†]Department of Radiology, University of Texas Southwestern Medical Center, Dallas, Texas 75235 [%]Department of Bioengineering, Penn State University, University Park, PA 16802 [¥]Department of Radiology, Leiden University Medical Center, Leiden, Netherlands [§]Department of Internal Medicine, University of Texas Southwestern Medical Center, Dallas, Texas 75235 [††]VA North Texas Health Care System, Dallas, Texas 75216 [**]Department of Chemistry, University of Texas at Dallas, Richardson, Texas 75083

Abstract

The role of diet and fat consumption in the pathogenesis of breast cancer is an important subject. We report on a method for non-invasive determination of lipid composition in human breast by proton MRS at 7T. Two respiratory-triggered TE-averaged STEAMs were performed on the adipose tissue of ten healthy volunteers where the second acquisition had all gradients inverted. This acquisition protocol allows for suppression of modulation side bands that complicate spectral analysis at the short TE_{avg} = 24.5 ms used. The entire acquisition takes approximately 10 minutes. Ten lipid peaks were typically resolved. T_1 and T_2 were also measured and used to correct the peak intensities. The average lipid composition calculated was saturated 28.7 ± 8.4%, monounsaturated 48.5 ± 7.9 %, and polyunsaturated 22.7 ± 3.1%, in close agreement with reported values from subcutaneous adipose measurements. Intra-subject variability was 2.0, 1.6, and 3.6% for the saturated, monounsaturated, and polyunsaturated fractions, respectively. In conclusion, we have shown that a chemical analysis of lipids in breast tissue can be determined quite simply, quickly, and non-invasively by proton MRS at 7T.

Keywords

adipose; NMR; MUFA; PUFA; TE-average; triglycerides

INTRODUCTION

Breast cancer screening and interventions have been increasingly successful in early detection and reduction of mortality rates. Prevention, however, is the most desirable goal. Some of the least expensive prevention options, dietary modification and omega-3 supplementation, may have a practical role in reducing the rates of breast malignancies. The interaction between fat consumption, fat composition, and the risk of cancer has been examined extensively. However, many of the studies reach conflicting conclusions. For example, epidemiological studies demonstrate high correlation between total fat

[1]Contact Information: Craig R. Malloy, University of Texas Southwestern Medical Center, Advanced Imaging Research Center, 5323 Harry Hines Blvd, NE4.2, Dallas, TX 75390-8568, Tel: 214-645-2720, Fax: 214-645-2744, Craig.Malloy@UTSouthwestern.edu.

consumption and breast cancer mortality (1,2). In addition to the amount of fat consumed, fat composition may also be a prognostic marker for tumorigenesis. Animal studies show that selected polyunsaturated fatty acids (PUFA) are associated with tumorigenesis (3,4). Conversely, protective effects have been attributed to α-linolenic and docosahexaenoic (DHA) acids (5), and ω-3 PUFA (6). Considerations of the lipodome as a complex composite marker consisting of 23 fatty acids have shown that a lipid profile low in linoleic acid and high in *cis*-monounsaturated fatty acids (MUFA) decreases the risks of breast cancer (7). Numerous negative results however have also been reported, where no significant association of fatty acid composition and breast cancer was found (8–10).

The discrepancies in some of the dietary intervention studies in humans may be due to limitations in the methodology used to evaluate dietary intake. Dietary records, dietary interviews, and food frequency questionnaires all suffer from subjectivity and unintentional under- or over-reporting. Since the chemical composition of adipose tissue reflects dietary fat over the preceding two years (11), noninvasive analysis of breast fat composition should provide an accurate index of the long-term effects of diet.

While magnetic resonance spectroscopy (MRS) has been previously used for evaluation of the water-(total) fat (W-F) ratio, there is ambiguity in the utility of this marker since some studies report elevated W-F ratios in malignant breast tissues (12,13), while others report no significant differences for benign and malignant breast lesions (14). The interpretation of this marker is complicated by partial volume contamination due to voxel placement, as well as by changes in T_2 of water rather than changes in the W-F ratios themselves (15). Indeed, fat is mostly perceived to be a nuisance in proton MRS, with most of the spectroscopic studies focusing on the detection of total choline-containing metabolites (tCho), since elevated tCho is an indicator of increased cell proliferation (16,17). *Ex vivo* breast fat composition has been quantified by MRS using ^{13}C (18) and while this method affords additional compositional information, as compared to proton MRS, it may be difficult to apply *in vivo* due to the high power requirement for proton decoupling. In the only *in vivo* MRS report on breast lipid composition, Dzendrowskyj et al. were able to measure changes in the allylic intensity throughout the menstrual cycle, but did not report on the PUFA/MUFA/saturated portions of the lipid (19), presumably due to the lack of spectral resolution in separating signals from these lipid fractions. In the present study, spectral resolution was improved by going to high fields thus allowing for baseline-resolution of most of the lipid peaks at 7T.

High field breast MRS can be technically challenging, particularly due to the large lipid peak at 1.3 ppm that can generate frequency modulation sidebands due to mechanical gradient vibrations. Two main methods have been developed to reduce these sidebands, namely the gradient polarity inversion scheme (20) and the TE-averaging scheme (21). These methods were combined in this study to allow for virtual elimination of this artifact from the spectra. Further challenge in high field human spectroscopy, the frequency and phase shifts due to respiration, was addressed using respiratory triggering in acquisition and coherent averaging in postprocessing (22).

Here, we report the use of high field proton MRS for non-invasive determination of lipid composition in female subjects. Normative values of PUFA, MUFA, and saturated fatty acids in the breast adipose tissue of ten healthy (without known breast disease) women are reported.

METHODS

The protocol was approved by the local Institutional Review Board. Informed consent was obtained from all participants prior to the study. Healthy young females (n = 10, age 26 ± 7 years; range 19 – 40; 4 Whites/1 Black/1 Asian/4 Hispanic subjects none of whom had diabetes or vascular disease. One individual was scanned 3 times for reproducibility. The subjects were in different phases of their menstrual cycle and had differing cup sizes. One had saline implants). All subjects were studied using a 7T whole-body system (Achieva, Philips Medical Systems, Cleveland, OH, USA). Volunteers were recumbent in a 45° right posterior oblique position with their backs resting against a blanket roll. Each volunteer's right arm was raised above her head and rested behind the head. Pillows were used to prop the head into a comfortable resting position. The left arm was rested on the left hip. One pillow was placed between the slightly bended knees and another pillow was placed between the ankles. This position was found to be very comfortable and reduced possible patient motion during the exam. For respiratory triggering, a pneumatic belt was put around the chest of the volunteers. A 10-cm diameter linear transmit/receive surface coil was positioned under the right breast and the breast was allowed to naturally lie on top of the coil. In cases of small breasts, the coil was propped up against the breast. The coil consists of a 1 mm-diameter silver wire segmented every 6 cm (λ/16) by 3.9 pF non-magnetic capacitors (ATC, Series B, Huntington Station, NY) and placed on a thin flexible Teflon former. Two variable capacitors (1–40 pF; Johansson, Camarillo, CA) were used for tuning and matching. The coil was padded with ~ 1 cm thick foam to reduce patient-induced losses by introducing a small distance between the poorly conductive human breast tissue and the coil (utilizing the so called lift-off effect (23)). The coil was SAR modeled using finite-difference time-domain (FDTD); in light of the fact that there are significant differences in lipid distribution within breast tissue, conservative SAR simulations were performed by placing the coil next to the heart, in which case highly conductive muscle tissue lies within the area of the maximum electric field of the coil. Using a TR of several seconds, both the time averaged and peak SAR values were much lower than the FDA limits. Heating tests on a human torso phantom were also performed to insure coil safety. After positioning the volunteers on their right side and placing the coil under the right breast, small (~150 mL) bags filled with D_2O were placed both in the central opening of the coil as well as on medial top of the breast, on the side opposite the coil, to improve B_0 and B_1 shimming (24). After positioning, the coil was tuned and matched, with typical matching of 35–40 dB. Three-plane T_2-weighted localization was performed to aid voxel placement. Second order localized shimming and frequency determination based on B_0 field mapping (using Shimtool) was then performed (25). Voxels, either 10×10×10 mm^3 (1mL) or 5×5×5 mm^3 (1/8 mL), were placed either in the outer regions of the breast or in fibroadipose areas within the breast that were visually determined to be predominantly composed of fat. For each voxel, two respiratory triggered STEAM acquisitions were performed where the second acquisition had all selection and dephasing gradients inverted. This was done in order to eliminate both frequency modulation sidebands caused by the large lipid peak at 1.3 ppm and eddy currents (20). The STEAM RF pulses were centered at 1.73 ppm. Each STEAM acquisition was a TE-averaged scan with four TE's −23 to 26 ms, with 16 averages per TE (21). A 16-step phase cycling was utilized. Other parameters were TM 20 ms, TR 2.5 s, no water suppression, BW 4 kHz, 4096 samples. The total scan time for the two STEAM series was about 10 min. T_1 (n = 2) and T_2 were measured (n = 3) using standard inversion recovery and echo-series sequences with TR = 6 s ($TR > 5 \times T_1^{longest}$). For the T_1 measurements 10 TI data points were acquired, and for the T_2 measurements 12 TE points were acquired. All volunteers tolerated the exam well. The individual STEAM spectra were coherently averaged (22) by first phasing them, referencing the dominant CH_2 peak to 1.3 ppm, and then adding all the spectra. Baseline correction was then performed and the spectra were fitted with Voigt lineshapes using ACD software (Toronto, Canada). Peaks were assigned and ratios calculated according to a

previous study (26). Briefly, we determined the lipid fractions as PUFA = F/E (see Figure 1 and Table 1 for the letter assignment), MUFA = 0.5*D/E – F/E, and saturated = (1 – PUFA – MUFA). In calculating the relaxation times, the T_2 data was normalized so that the first point (at TE = 23 ms) was scaled to one. The T_1 data was normalized so that the final point is at one. Relaxation curves were fitted using a three-parameter non-linear least-squares fit based on Levenberg-Marquardt algorithm (*curvefit*) in IDL (RSI, Boulder, CO).

RESULTS

A typical spectrum from the fibroadipose fraction of the breast is shown in Figure 1. Ten lipid peaks (A–J) were normally resolved with the methine glycerol backbone protons at 5.22 ppm often appearing as a shoulder on the methine protons of the double bond at 5.31 ppm, see Table 1. No choline (3.22 ppm) was detected in any of the subjects. The water signal was also barely detectable in most cases. The diallylic proton peak F at 2.77 ppm, which is used in the calculation of the PUFA fraction, is fully baseline resolved. The D and E peaks at 2.03 and 2.25 ppm, used for calculation of the MUFA fraction and for overall normalization, respectively, while not baseline resolved are well separated and thus allow for confident fitting with Voigt lineshapes. Using peaks D, E, and F in the calculation of the lipid fractions (26), the average lipid composition determined from all ten subjects was saturated = 28.7 ± 8.4%, MUFA = 48.5 ± 7.9 %, and PUFA = 22.7 ± 3.1%, see Table 2. The standard deviation reported is the inter-subject deviation. The reproducibility of the measurement was evaluated by examining the same subject on three different occasions, with several weeks between exams. We obtained intra-subject variability of 2.0, 1.6, and 3.6 % for the saturated, MUFA, and PUFA lipids, respectively. Since the three exams of the same subject were not scheduled to fall on a specific day within the menstrual cycle, and because metabolic composition may depend on the cycle, the actual inter-subject variability may differ from these reported values. All fractional values were corrected for relaxation using the measured values of T_1 and T_2, see Table 1 and Figure 2.

The importance of respiratory triggering the scan is shown in Fig. 3A. Pronounced fluctuations caused by changes in the susceptibility of the expanding lungs during breathing are seen if triggering is not applied. Although these fluctuations can be removed by postprocessing, this complicates the analysis of the data and was easily avoided by triggering. In addition to respiratory triggering, coherent averaging was beneficial in improving spectral resolution. In some cases, the full width at half max (FWHM) was narrowed from 32 Hz in standard averaging to 24 Hz in coherent averaging. This additional spectral resolution aids in better fitting of the data. Another methodological modification of the acquisition protocol was the use of two acquisitions – one with the positive encoding/dephasing gradient directions and a second acquisition with their inverted (negative) counterparts. The sum of these two acquisitions allows the suppression of artifacts from modulation sidebands and eddy currents (20). Figure 3B shows the improvement in the overall peak symmetry upon the addition of the positive and negative gradient acquisitions. Arrows show (blue line) the unleveled appearance of the acquisition using the positive gradients only. Similar but reversed uneven appearance is seen for the negative gradients only (dark red line). The sum of the two (black line) removes this unevenness, thus removing the associated artifacts. Although this unevenness is visually observed only for the largest CH_2 peak at 1.3 ppm, it will be present, in scaled magnitude, for all of the peaks. Without its removal, incorrect fitting of the spectra may occur.

Special attention was also paid to the additional removal of the modulation side bands arising from the dominant CH_2 peak at 1.3 ppm. Figure 3C shows the artifactual baseline around 3.1 ppm (and its anti-symmetric, with respect to the large peak at 1.3 ppm, appearance at −0.5 ppm, both shown in thin black arrows; delta = 3.1-1.3 = 1.8 ppm; There

is also a less visible modulation side band that is 0.9 ppm (i.e. 1.8/2 = 0.9 ppm) away from the dominant 1.3 ppm peak. This peak thus appears at 0.4 ppm and 2.2 ppm, in orange thick arrows). These artifacts could potentially increase the errors in peak measurement in two ways. First, the sidebands that are 1.8 ppm away from CH_2 infringe with proper baseline correction of the spectra, thus contributing to improper line fitting during quantification. More importantly, the sidebands that are 0.9 ppm away from CH_2 directly overlap the peaks of interest thus skewing the final results. The use of four different TE's that are separated by 1 ms modulated the phase of this artifact such that it approximately cycled through phases of θ, θ + 90, θ + 180, and θ + 270 degrees, where θ is an arbitrary initial phase. The addition of the four spectra then resulted in clean cancellation of the modulation sidebands, Figure 3D.

DISCUSSION

The mean values of the relative fat fractions in breast adipose tissue (Table 2), appear to be similar (± 1–2%) to the lipid composition of calf subcutaneous fat (26) as measured by a similar MRS protocol. This is not surprising given reports of the small differences of fat composition of different fat depots in *ex vivo* human samples (27). Comparison of our results with that of a large study on 104 biopsied women (28) shows similar fractions of saturated (29% in our study vs. 30% in that study), and PUFA (23% vs. 19%) fats, with the fraction of MUFA acids differing somewhat (48% vs. 40%). Given the extended range for MUFA acids that we find in our study (40 – 65 %), and given the small sample size (n = 10), it may be that the average value reported here is factual. However, given that the MUFA fraction is calculated as 0.5*D/E – F/E, the higher reported MUFA fraction in our study can be a consequence of systematic over-fitting of peak D due to potential underestimation of the tails of the dominant CH_2 peak at 1.3 ppm. As seen from the individual Voigt fits in figure 1, the tails of the large 1.3 ppm peak extend in the region of peak D, possibly contributing up to 4–5% of its intensity. Fitting of the data using the reported multiplet structure of the individual triglycerides (29) rather than fitting with singlets may improve the reliability of the fit. Another potential source of error in quantifying the lipid fractions is the chemical shift displacement. Given that the bandwidth of the STEAM shaped RF pulses was 2.94 kHz (B_{1max} = 20 μT, RF pulse duration 4.81 ms), the acquisition voxel for peak F at 2.77 ppm was shifted less than 10% of the overall voxel dimensions with respect to peak D at 2.04 ppm. This amounts to a shift of about 0.5 mm. We thus tried to always position the voxel so as to leave a small margin of homogeneous lipid surrounding it. We estimate that chemical shift displacement errors were negligible in our protocol.

Table 1 reports the T_1 and T_2 values and the experimental relaxation curves for the three peaks (D, E, and F) used in the calculation of the lipid composition are shown on Figure 2. As seen in figure 2A, the first T_1 data point (at TI = 6 ms) is not at −1.0 due to both imperfect inversion and to signal decay during the inversion time. The T_1 fits however were generally satisfactory. Comparing the T_1 of the fibroadipose breast fat to that of the calf subcutaneous fat (26) we find differences ([breast – calf]/calf) of −1% (for peak A), 4% (B), 47% (C), 29% (D), 16% (E), and 8% (F). Comparing the T_2 of breast and calf lipids we find differences of −39% (for peak A), −17% (B), +32% (C), −18% (D), −34% (E), and −31% (F). The large differences in the relaxation times may reflect true differences in the milieu, or they may be an artifact from fitting the data, due to the fact that the overall shim of the calf subcutaneous fat was better than the shim in the breast thus increasing the uncertainty in fitting the separate peaks in the beast. The combined influence of the T_1 and T_2 correction on the fat composition amounted to (for the experimentally used TE_{avg} = 24.5 ms and TM = 20 ms) a decrease by 1.7% in the PUFA fraction, an increase by 4.3% for the MUFA, and a decrease by 2.7% in the saturated fraction, as compared to the uncorrected values. Given the small standard deviations of the measured relaxation times, and the time cost of measuring

them, per subject, only the population-averaged T_1 and T_2 values were used in these corrections.

Figure 1 clearly demonstrates the ability to non-invasively probe the fibroadipose breast tissue using a 10-cm diameter surface coil at 7T. The B_1 profile of the coil is highly inhomogeneous and the useful coil coverage was limited to a depth of approximately 6 cm, with lateral coverage of approximately 10 cm. While this coverage was sufficient for this pilot study, multi-transmit, phased array, or TEM strip coils may have to be designed if bilateral and axillary coverage is desired. A simple bilateral coil has already been shown to have a good overall coverage for 7T breast MRI (30). Without currently having the option of multi-transmit, we used small D_2O bags positioned on the side of the breast opposite the coil to shift the B_1 field deeper into the fibroadipose tissue (24).

CONCLUSIONS

In vivo determination of the relative proportions of saturated, MUFA and PUFA fractions of human fibroadipose breast tissue is possible using proton MRS at 7T. This methodology will allow for the non-invasive quantification of lipid composition to aid studies on nutritional and supplemental intervention and their effect on breast cancer predisposition.

Acknowledgments

This work was supported by the National Center for Research Resources (RR02584) and the Department of Defense (W81XWH-06-2-0046).

References

1. Bagga D, Capone S, Wang HJ, Heber D, Lill M, Chap L, Glaspy JA. Dietary modulation of omega-3/omega-6 polyunsaturated fatty acid ratios in patients with breast cancer. J Natl Cancer Inst. 1997; 89(15):1123–1131. [PubMed: 9262250]
2. Godley PA. Essential fatty acid consumption and risk of breast cancer. Breast Cancer Res Treat. 1995; 35(1):91–95. [PubMed: 7612909]
3. Chan PC, Ferguson KA, Dao TL. Effects of different dietary fats on mammary carcinogenesis. Cancer Res. 1983; 43(3):1079–1083. [PubMed: 6825080]
4. Cohen LA, Thompson DO, Maeura Y, Choi K, Blank ME, Rose DP. Dietary fat and mammary cancer. I. Promoting effects of different dietary fats on N-nitrosomethylurea-induced rat mammary tumorigenesis. J Natl Cancer Inst. 1986; 77(1):33–42. [PubMed: 3459924]
5. Maillard V, Bougnoux P, Ferrari P, Jourdan ML, Pinault M, Lavillonniere F, Body G, Le Floch O, Chajes V. N-3 and N-6 fatty acids in breast adipose tissue and relative risk of breast cancer in a case-control study in Tours, France. Int J Cancer. 2002; 98(1):78–83. [PubMed: 11857389]
6. Chajes V, Bougnoux P. Omega-6/omega-3 polyunsaturated fatty acid ratio and cancer. World Rev Nutr Diet. 2003; 92:133–151. [PubMed: 14579688]
7. Bougnoux P, Giraudeau B, Couet C. Diet, cancer, and the lipidome. Cancer Epidemiol Biomarkers Prev. 2006; 15(3):416–421. [PubMed: 16537692]
8. Eid A, Berry EM. The relationship between dietary fat, adipose tissue composition, and neoplasms of the breast. Nutr Cancer. 1988; 11(3):173–177. [PubMed: 3405869]
9. London SJ, Sacks FM, Stampfer MJ, Henderson IC, Maclure M, Tomita A, Wood WC, Remine S, Robert NJ, Dmochowski JR, et al. Fatty acid composition of the subcutaneous adipose tissue and risk of proliferative benign breast disease and breast cancer. J Natl Cancer Inst. 1993; 85(10):785–793. [PubMed: 8487323]
10. Petrek JA, Hudgins LC, Levine B, Ho M, Hirsch J. Breast cancer risk and fatty acids in the breast and abdominal adipose tissues. J Natl Cancer Inst. 1994; 86(1):53–56. [PubMed: 8271285]
11. van Staveren WA, Deurenberg P, Katan MB, Burema J, de Groot LC, Hoffmans MD. Validity of the fatty acid composition of subcutaneous fat tissue microbiopsies as an estimate of the long-term

average fatty acid composition of the diet of separate individuals. Am J Epidemiol. 1986; 123(3): 455–463. [PubMed: 3946391]

12. Jagannathan NR, Singh M, Govindaraju V, Raghunathan P, Coshic O, Julka PK, Rath GK. Volume localized in vivo proton MR spectroscopy of breast carcinoma: variation of water-fat ratio in patients receiving chemotherapy. NMR Biomed. 1998; 11(8):414–422. [PubMed: 10221584]
13. Sijens PE, Wijrdeman HK, Moerland MA, Bakker CJ, Vermeulen JW, Luyten PR. Human breast cancer in vivo: H-1 and P-31 MR spectroscopy at 1. 5 T. Radiology. 1988; 169(3):615–620. [PubMed: 2847230]
14. Roebuck JR, Cecil KM, Schnall MD, Lenkinski RE. Human breast lesions: characterization with proton MR spectroscopy. Radiology. 1998; 209(1):269–275. [PubMed: 9769842]
15. Manton DJ, Chaturvedi A, Hubbard A, Lind MJ, Lowry M, Maraveyas A, Pickles MD, Tozer DJ, Turnbull LW. Neoadjuvant chemotherapy in breast cancer: early response prediction with quantitative MR imaging and spectroscopy. Br J Cancer. 2006; 94(3):427–435. [PubMed: 16465174]
16. Bolan PJ, Nelson MT, Yee D, Garwood M. Imaging in breast cancer: Magnetic resonance spectroscopy. Breast Cancer Res. 2005; 7(4):149–152. [PubMed: 15987466]
17. Haddadin IS, McIntosh A, Meisamy S, Corum C, Styczynski Snyder AL, Powell NJ, Nelson MT, Yee D, Garwood M, Bolan PJ. Metabolite quantification and high-field MRS in breast cancer. NMR Biomed. 2009; 22(1):65–76. [PubMed: 17957820]
18. Victor TA, Bergman A, Knop RH. Detecting fatty acids of dietary origin in normal and cancerous human breast tissue by 13C nuclear magnetic resonance spectroscopy. Br J Cancer. 1993; 68(2): 336–341. [PubMed: 8347488]
19. Dzendrowskyj TE, Noyszewski EA, Beers J, Bolinger L. Lipid composition changes in normal breast throughout the menstrual cycle. MAGMA. 1997; 5(2):105–110. [PubMed: 9268073]
20. Dong Z, Dreher W, Leibfritz D. Experimental method to eliminate frequency modulation sidebands in localized in vivo 1H MR spectra acquired without water suppression. Magn Reson Med. 2004; 51(3):602–606. [PubMed: 15004803]
21. Bolan PJ, DelaBarre L, Baker EH, Merkle H, Everson LI, Yee D, Garwood M. Eliminating spurious lipid sidebands in 1H MRS of breast lesions. Magn Reson Med. 2002; 48(2):215–222. [PubMed: 12210929]
22. Gabr RE, Sathyanarayana S, Schar M, Weiss RG, Bottomley PA. On restoring motion-induced signal loss in single-voxel magnetic resonance spectra. Magn Reson Med. 2006; 56(4):754–760. [PubMed: 16964612]
23. Suits BH, Garroway AN, Miller JB. Surface and gradiometer coils near a conducting body: the lift-off effect. J Magn Reson. 1998; 135(2):373–379. [PubMed: 9878466]
24. Douglas, D.; Dimitrov, IE.; Ren, J.; Sherry, AD.; Malloy, CR. Extending the Sensitivity Volume of Surface Coils for Spectroscopy at 7T by Using Deuterium Water Bags. Proceedings of the Annual Meeting of ISMRM; Stockholm, Sweden. 2010. p. 3310
25. Schär, M.; Kozerke, S.; Boesiger, P. Considerations on shimming for cardiac applications at 1.5 and 3.0T. Proceedings of the 11th Annual meeting of ISMRM; Toronto, Canada. 2003. p. 174
26. Ren J, Dimitrov I, Sherry AD, Malloy CR. Composition of adipose tissue and marrow fat in humans by 1H NMR at 7 Tesla. J Lipid Res. 2008; 49(9):2055–2062. [PubMed: 18509197]
27. Calder PC, Harvey DJ, Pond CM, Newsholme EA. Site-specific differences in the fatty acid composition of human adipose tissue. Lipids. 1992; 27(9):716–720. [PubMed: 1487971]
28. Petrek JA, Hudgins LC, Ho M, Bajorunas DR, Hirsch J. Fatty acid composition of adipose tissue, an indication of dietary fatty acids, and breast cancer prognosis. J Clin Oncol. 1997; 15(4):1377–1384. [PubMed: 9193329]
29. Guillen M, Ruiz A. Edible oils: discrimination by 1H nuclear magnetic resonance. J Sci Food Agric. 2003; 88:338–346.
30. Warmington, L.; Adriany, G.; Snyder, C.; Auerbach, E.; Bolan, PJ. 7T breast imaging with a 2-channel bilateral loop design. Proceedings of the 17th Annual meeting of ISMRM; Hawaii, US. 2009. p. 3006

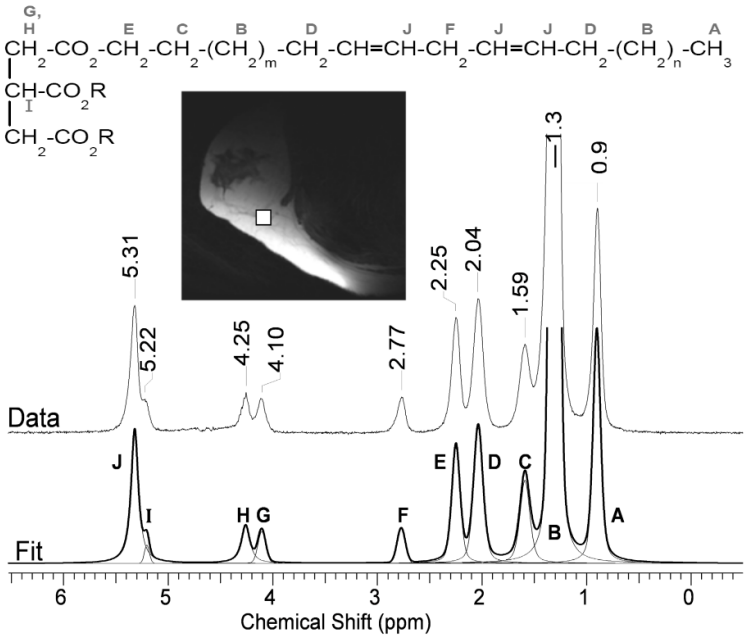

FIG. 1.

Proton NMR spectrum of the breast adipose tissue of a 19 year old volunteer at 7T. Ten resonances (A–J) are typically resolved. The letter assignment on the spectrum is also shown on the corresponding chemical structure of a triglyceride. The bottom trace shows the overall fitted spectrum (thick line) composed of the individual Voigt peaks (thin lines). The upper trace is the acquired data. The insert shows a T_2-weighted image of the position of the spectral voxel in the breast.

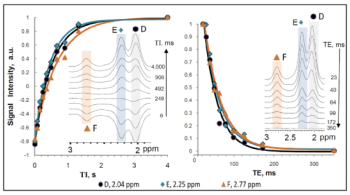

FIG. 2.

Relaxation curves and fits. For clarity of presentation, only data for D, E, and F is shown as these are the peaks used in the calculation of lipid composition. **A.** Inversion recovery curves for measuring T_1. The TI values used were 6, 77, 157, 249, 358, 492, 664, 906, 1318, and 4000 ms with a constant TR = 6 s. **B.** TE-decay curves for measuring T_2. TE values used were 23, 31, 40, 51, 64, 79, 99, 126, 172, and 350 ms with a constant TR = 6 s.

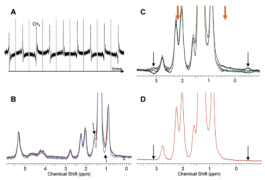

FIG. 3.

Methods for improving spectral quality of breast MRS at 7T. **A**. Signal fluctuation when no respiratory triggering is used. The individual time points are 3 – 5 s apart. Triggering the acquisition removes this fluctuation. **B.** Eddy currents and modulation sidebands can cause uneven presentation of the spectra for either positive (blue line, arrows) or negative (brown line) acquisition. The addition of the two (black line) removes the artifacts. **C.** Modulation sidebands (arrows) appear anti-symmetrically around the large CH_2 peak at 1.3 ppm. The phase of the bands changes as the TE is changed in steps of 1 ms (different colors). **D.** TE-averaging of the four spectra from C. reduces significantly the sidebands.

Table 1

Chemical shift assignment and relaxation times of fat protons in adipose breast tissue.

Letter and Structure	Chemical Group	Chemical Shift, ppm	T_1, ms	T_2[a], ms
A (methyl protons)	-C**H**$_3$	0.90	1,071 ± 27	41 ± 18
B (methylene protons)	-(C**H**$_2$)$_n$-	1.30	549 ± 16	52 ± 17
C (methylene protons β to COO)	-C**H**$_2$-CH$_2$-COO	1.59	470 ± 15	40 ± 8
D (methylene protons α to C=C)	-C**H**$_2$-CH=CH-C**H**$_2$-	2.04	502 ± 11	32 ± 4
E (methylene protons α to COO)	-C**H**$_2$-COO	2.25	465 ± 22	36 ± 3
F (diallylic methylene protons)	=CH-C**H**$_2$-CH=	2.77	629 ± 72	40 ± 3
G (methylene glycerol backbone)	C**H**$_2$-O	4.10		
H (methylene glycerol backbone)	C**H**$_2$-O	4.25		
I (methine glycerol backbone)	C**H**-O	5.22		44
J (methine protons)	-C**H**=C**H**-	5.31		42 ± 19

Resonance assignments by letter correspond to Figure 1. Values are mean ± 1 SD.

[a] Apparent T_2; Although the decay curves were fitted with single exponential, there may be additional J-coupling contributions to the decay.

Table 2

Fat composition of fibroadipose breast tissue

Lipid Fraction	Mean % ± SD	Range %	Intra-subject variability %
Saturated	28.7 ± 8.4	14 – 38	2.0
MUFA	48.5 ± 7.9	40 – 65	1.6
PUFA	22.7 ± 3.1	19 – 29	3.6